Nat Hazards
DOI 10.1007/s11069-010-9684-5

ORIGINAL PAPER

# Simulation of the Hurricane Dennis storm surge and considerations for vertical resolution

**Dmitry S. Dukhovskoy · Steven L. Morey**

Received: 1 April 2010 / Accepted: 2 December 2010


**Abstract** A high-resolution storm surge model of Apalachee Bay in the northeastern Gulf of Mexico is developed using an unstructured grid finite-volume coastal ocean model (FVCOM). The model is applied to the case of Hurricane Dennis (July 2005). This storm caused underpredicted severe flooding of the Apalachee Bay coastal area and upriver inland communities. Accurate resolution of complicated geometry of the coastal region and waterways in the model reveals processes responsible for the unanticipated high storm tide in the area. Model results are validated with available observations of the storm tide. Model experiments suggest that during Dennis, excessive flooding in the coastal zone and the town of St. Marks, located up the St. Marks River, was caused by additive effects of coincident high tides ($\sim$10–15% of the total sea-level rise) and a propagating shelf wave ($\sim$30%) that added to the locally wind-generated surge. Wave setup, the biggest uncertainty, is estimated on the basis of empirical and analytical relations. The Dennis case is then used to test the sensitivity of the model solution to vertical discretization. A suite of model experiments is performed with varying numbers of vertical sigma ($\sigma$) levels, with different distribution of $\sigma$-levels within the water column and a varying bottom drag coefficient. The major finding is that the storm surge solution is more sensitive to resolution within the velocity shear zone at mid-depths compared to resolution of the upper and bottom layer or values of the bottom drag coefficient.

**Keywords** Storm surge modeling · Unstructured grid · Vertical discretization · Coastal inundation

## 1 Introduction

The coastal zone of Apalachee Bay in the northeastern Gulf of Mexico is susceptible to intense flooding during storms. The largest recorded surge in the area was the "Great North

D. S. Dukhovskoy (✉) · S. L. Morey
Florida State University, Center for Ocean-Atmospheric Prediction Studies, Tallahassee, FL 32306-2840, USA
e-mail: ddukhovskoy@fsu.edu

Published online: 23 December 2010

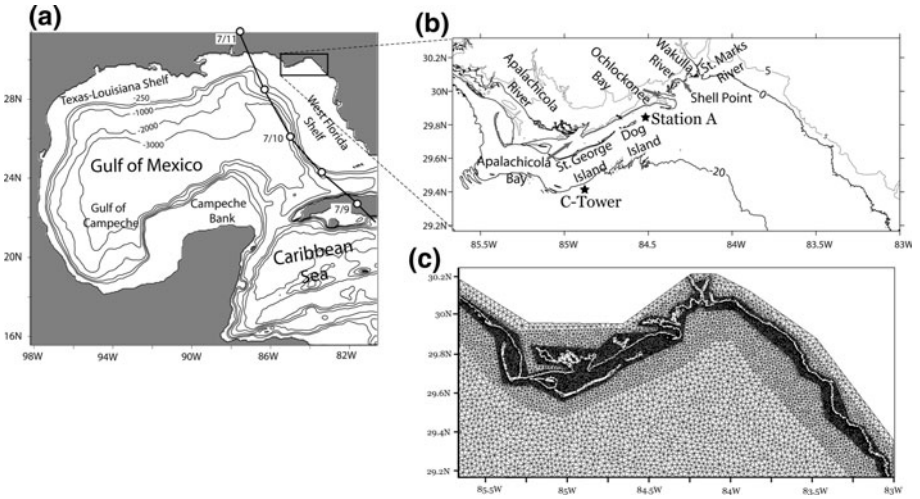


**Fig. 1** **a** The domain of the coarse-resolution NCOM described in Morey et al. (2006) includes the Gulf of Mexico and western Caribbean Sea. The domain of the high-resolution model encompasses the Apalachee Bay region (*small box*) and is nested in the coarse model. The Hurricane Dennis track is shown with a *black line* with storm locations every 12:00 UTC. **b** Map of Apalachee Bay region. The −20-, 0- and 5-m levels are contoured. The locations of NOAA NDBC station SGOF1 ("C-Tower") and NOAA NGI station A are shown. **c** Unstructured mesh of the Apalachee Bay region. The size of the triangular elements decreases as approaching to the coast line (*white curve*). The southern and western sides of the domain are lateral open boundaries

Florida Storm" (September 1873), which made landfall along the Apalachee Bay coast and caused a storm tide of 6.1 m at the St. Marks Lighthouse (Fig. 1) and 5.5 m in the town of St. Marks, located about 10 km up the St. Marks River (Tallahassee Weekly Floridian, September 23, 1873). Luckily, no hurricane has made landfall directly in the region over the past several decades, though several tropical storms have hit the area. However, the region has been impacted by severe flooding associated with storms making landfall farther to the west along the Florida Panhandle region. In July 2005, Hurricane Dennis made landfall at Santa Rosa Island and caused unexpected serious inundation of the coastal zone of Apalachee Bay, including underpredicted flooding in the town of St. Marks, approximately 275 km to the east of the landfall location (FDEP 2006). The failure of forecasts to anticipate this high surge raised several questions among the surge modeling community about the validity and reliability of storm surge forecasting methods used at the time.

Morey et al. (2006) addressed the problem of the unexpected flooding along Apalachee Bay during Hurricane Dennis. They employed a 1/60° resolution model of the Gulf of Mexico based on the Navy Coastal Ocean Model (NCOM) forced by an observationally derived hurricane wind product. The major finding of Morey et al. (2006) is that the hurricane, which tracked for several days almost parallel to the West Florida coast (Fig. 1a), generated a shelf wave that contributed significantly to the locally wind-forced surge in Apalachee Bay. The relatively simple dynamical explanation is that along-coast winds persisting for roughly more than an inertial period will result in across-shelf transport to the right of the wind. Thus, southerly winds east of the storm center built a high sea-level anomaly along the West Florida coast that began propagating northward as a topographic Rossby (or shelf) wave. The high sea-level anomaly was reinforced as it propagated northward by the hurricane translating at a similar speed. Although the

localized winds at such a long distance from the storm's center were not strong enough to produce the extreme flooding experienced in the area, the remotely generated wave resulted in approximately 30% of additional sea-level rise in the bay. Surge models with a local model domain not accounting for these remote influences are not able to accurately predict the surge from this storm.

The Gulf of Mexico model employed in this previous study was not designed to accurately resolve the locally complex geometry of the coastline and was not able to replicate the localized spatial variability and amplification of the storm surge in the area. Additionally, this work relied on a two-dimensional model, and Weisberg and Zhang (2008) have shown that using a three-dimensional model can significantly impact the solution. Morey et al.'s (2006) work was primarily focused on providing a dynamical explanation to the unexpectedly high surge and generation mechanisms of the shelf wave rather than accurate simulation of storm surge along the coast. Thus, the simulated storm surge in Apalachee Bay was not thoroughly verified with observations. A simple comparison with the reported surge height at Shell Point (Fig. 1b) indicates that the Morey et al. (2006) simulation underpredicts the surge by 0.8 m ($\sim$35%) and does not resolve small-scale coastal features such as river channels that are critical to the still unexplained flooding of the town of St. Marks (FEMA 2005). The first part of this new work is a continuation of Morey et al.'s (2006) study, which (1) presents a high-resolution surge model of Apalachee Bay that accurately resolves coastline and river channels and (2) analyzes and compares model results with observations.

A high-resolution Apalachee Bay surge model is developed (referenced further in the text as the Apalachee Bay model). The model is based on the unstructured grid Finite-Volume Coastal Ocean Model (FVCOM) of Chen et al. (2003), which includes wetting and drying. The various factors responsible for the coastal inundation, in addition to the wind-driven surge (atmospheric pressure contributions, wave setup, and astronomical tides), are estimated to assess and validate the simulation against observations of the storm tide, which is the total observed sea-level rise above mean sea level (MSL) during a storm (whereas storm surge is used as a term to describe the sea-level rise above the predicted astronomical tide). The Apalachee Bay model is applied to the case of Hurricane Dennis. The results are analyzed to further explain the dynamics responsible for the unexpected surge and the localized amplification and variability of the flooding. Verification of the results with observed sea-level observations and high-water marks demonstrates the utility of the model and storm tide estimation methodology.

The second part of the paper is focused on the sensitivity of the storm surge solution to vertical discretization of the water column. Although 2D surge models have been used for several decades for storm surge studies (e.g., Platzman 1958; Jelesnianski 1965; Mattocks and Forbes 2008; Rao et al. 2009), the utility of 3D versus 2D surge models has been demonstrated in a number of studies (e.g., Murty 1984; Weisberg and Zheng 2006, 2008). The major drawback of a simplified vertically averaged surge model is its physically inaccurate parameterization of the bottom friction. To overcome this problem, the bottom stress can be fine-tuned or a one-dimensional model that locally calculates the bottom stress can be added to a 2D model (Welander 1957; Jelesnianski 1970; Nihoul 1977). However, even if the bottom stress coefficient is properly parameterized, a 2D model does not resolve the vertical flow structure. Depth-average velocity does not represent the real near-bottom velocity well since the flow structure can have strong shear between the upper and lower layers in the shallow regions, even in unstratified shallow water, as will be shown in this paper. Also, tuning of a 2D model cannot be done for the forecast run and

involves other uncertainties (see detailed analysis of 2D ADCIRC hindcast of Hurricane Katrina case, in Weisberg and Zhang 2008).

A logical progression from previous studies of the 2D versus 3D approach is to examine the sensitivity of storm surge models to vertical resolution. Understanding this sensitivity can allow optimization of storm surge models for accuracy and computational efficiency. In this study, a suite of model experiments is run to understand how the model solution responds to the number and distribution of vertical levels in a $\sigma$-coordinate, or terrain-following, model. Results from these experiments, and additional experiments in which the bottom drag coefficients are modified, illustrate that the surge solution is sensitive to resolution within a zone of high shear that can occur in shallow water under high-wind scenarios and is less sensitive to resolution of the near-surface and near-bottom layers.

## 2 Numerical model description

FVCOM, a time-dependent, three-dimensional, primitive equation, unstructured grid numerical ocean model, is configured for the Apalachee Bay region from 85°40′W to 83°2′W and 29°10′N to 30°15′N (Fig. 1b). Topography of the region is derived from the 3 arc-second ($\sim$90 m) resolution gridded database of the National Geophysical Data Center (NGDC) (Divins, D.L., and D. Metzger, NGDC Coastal Relief Model, www.ngdc.noaa.gov/mgg/coastal/coastal.html).

In this study, FVCOM is used as a three-dimensional model with a sigma ($\sigma$) vertical coordinate system. The first part of the paper analyzes results from a 10 $\sigma$-level configuration of the model ("10-s" experiment in Table 1). For sensitivity tests discussed in Sect. 7, the model is run with a varying number and a varying distribution of $\sigma$-levels. One experiment is run with a modified calculation of the bottom stress (Table 1) described in Sect. 7. A 2D model simulation is also run for comparison with previous studies.

**Table 1** Model experiments

| Experiments | Description |
|---|---|
| 10-s, 9-s, 8-s, …, 4-s | 10, 9, 8, …, 4 evenly distributed $\sigma$-levels. Forcing: wind stress and sea elevation at the OB (from NCOM simulation by Morey et al. 2006) |
| nw10-s | Twin experiments with 10-s but with no wind (only shelf wave incoming at the OB) |
| wnd10-s | Twin experiments with 10-s but with wind forcing only |
| 2D | Two-dimensional configuration. Same forcing as in 10-s, …, 4-s experiments |
| 61-s | 6 $\sigma$-levels distributed such that the 1st level is at the surface, the 2nd level is at the middle of the water column and the rest levels are distributed in the lower half of the water column. Same forcing as in 10-s, …, 4-s experiments. $\sigma$-coordinates of the vertical levels: [0, −0.46, −0.77, −0.92, −0.98, −1]. |
| 40-s | Same as 4-s but $C_d$ is calculated as in 10-s. Same forcing as in 10-s, …, 4-s experiments |
| 70-s | Same as 7-s but $\sigma$-levels are distributed such that the shear zone is poorly resolved and both bottom and surface slabs are well resolved $\sigma$-layers. $\sigma$-coordinates of the vertical levels: [0, −0.09, −0.26, −0.5, −0.74, −0.91, −1]. |
| 71-s | Same as 7-s but $\sigma$-levels are distributed such that the shear zone is well resolved and bottom and surface slabs are resolved with 1 $\sigma$-layer each. $\sigma$-coordinates of the vertical levels: [0, −0.36, −0.44, −0.5, −0.56, −0.64, −1]. |

The bottom stress is parameterized by a quadratic law with drag coefficient calculated from logarithmic bottom layer (see Sect. 7 for more detail). For mathematical closure of the primitive equations, the Smagorinsky horizontal diffusion parameterization method is applied (Smagorinsky 1963). The vertical eddy viscosity is approximated by the Mellor and Yamada (1982) level 2.5 turbulent closure model. The computational time step varies from 0.05 through 0.25-s for the external mode and 0.25–2.5-s for the internal mode, depending on the minimum thickness of the $\sigma$-layers. The model equations and additional numerical details can be found in Chen et al. (2003, 2006, 2007).

For the applications described here, the horizontal grid is prepared with the unstructured mesh generator "Triangle" developed by Shewchuk (2002). The method is based on a conforming Delaunay triangulation that triangulates a set of points such that no point in the given set falls in the interior of the circumcircle of any triangle element. In this triangulation, additional points (Steiner points) can be added to the original set to meet constraints on the minimum angle and maximum triangle area. The Apalachee Bay model grid has a total of 40,955 triangular elements with 20,588 nodes (Fig. 1c). The model grid has 3 regions of different resolutions. Near the coastal region, the smallest edge of a triangle element is 25 m, and most of the elements have edges $\sim$100 m. Away from the coastal region is a zone with coarser resolution and the largest edge is 4 km (Fig. 1c). In the offshore region adjacent to the open western and southern boundaries, the resolution degrades more with the largest edge of an element of 6 km.

The FVCOM Apalachee Bay model is forced at the surface by the wind stress used in the Morey et al. (2006) Gulf of Mexico simulation. Wind fields are constructed for the time period 00:00 UTC 8 July—23:00 10 July UTC 2005, by applying an objective gridding method (Morey et al. 2005) to combine data from the NOAA AOML Hurricane Research Division Wind Analyses (H*Wind fields, Powell et al. 1998) and the National Centers for Environmental Prediction Reanalysis II (NCEPR2) winds. Stress is calculated on the basis of bulk aerodynamic formulae with a Large et al. (1994) drag coefficient as in Morey et al. (2005). The H*Wind fields provide 1-min maximum sustained winds over a region centered about the hurricane on a 6-km grid roughly 960 km by 960 km. The objective gridding technique essentially forms a complete wind field over the model domain by filling in the region not covered by the H*Wind fields with NCEPR2 winds in a smooth and physically sound manner. It is noteworthy that the models experiments described here are not forced by atmospheric pressure, but the impact of the atmospheric pressure on the sea level is added to the simulated storm surge estimates for comparison to observational data (Sect. 4.1).

The Apalachee Bay model is nested into the coarser-resolution Gulf of Mexico model of Morey et al. (2006). Using this nesting approach, the Apalachee Bay model simulates surge due to the local wind as well as the remotely forced incoming long shelf wave (topographic Rossby wave). Other possible contributions to the flooding such as tides, river discharge, wind waves, and the inverse barometer effect are not simulated and are assumed to be dominantly linearly additive for this problem. The Apalachee Bay model is integrated from rest, forced at the surface and lateral open boundaries for 70.5 h, from 00:00 UTC 8 July to 22:30 UTC 10 July 2005. For identifying the role of different factors contributing to the coastal inundation, two other experiments are run in addition to the realistically forced simulation. One experiment is run with wind stress only with no forcing at the lateral boundaries ("wnd10-s", Table 1), and the other is forced only at the lateral open boundaries with no wind forcing, allowing for free propagation of the long shelf wave ("nw10-s", Table 1).

## 3 Simulation results

Major features of the simulated sea surface elevation in the high-resolution Apalachee Bay model (Fig. 2) are similar to the previous storm surge solutions obtained from the Gulf of Mexico model of Morey et al. (2006). A long shelf wave generated by persistent alongshore winds along the West Florida Shelf (WFS) enters the domain from the southern boundary and propagates along the shelf to the western boundary. As shown in the previous study, this wave contributes substantially ($\sim$30%) to the local wind-driven surge along the northern part of the bay. However, this new FVCOM simulation reveals local amplifications of the storm surge near the coast and in the small bays that are absent in the study with the coarser Gulf of Mexico numerical simulation. The largest sea-level response to the storm in the model occurs after 18:00 UTC 10 July, as the storm's winds turn locally onshore and the crest of the long shelf wave generated along the West Florida Shelf arrives in the northern Apalachee Bay area. At this time, the Apalachee Bay model predicts large sea surface elevation gradients and a markedly higher surge along the coast than the previous model study.

The previous Gulf of Mexico model predicted high storm surge (>1.3 m) in the Ochlockonee Bay–St. Marks River area with local maximum of 1.39 m in the vicinity of Ochlockonee Bay. High storm surge (>1.9 m) occurs in the same region in the finer-resolution Apalachee Bay model (Upper panel, Fig. 3), but the local maximum surge in the Apalachee Bay model is increased by 75% (2.43 m) and is shifted up the St. Marks and Wakulla rivers. In this simulation, the surge has propagated $\sim$17 km up the Wakulla River and the St. Marks River and is amplified to over 2.4 m from 2 m at the Apalachee Bay coast. This is likely the manifestation of the funneling effect, which is the amplification of the surge energy in a coastal region due to a specific (triangular) shape of a coast (As-Salek 1998). In the St. Marks–Wakulla rivers case, topographic isolines converge forming "V"-shaped valleys that are ideal for promoting the funneling effect.

## 4 Storm tide estimation

The surge model forced only by wind stress and perturbations in the barotropic flow at the lateral boundaries predicts the sea-level rise due to the locally wind-driven surge and the

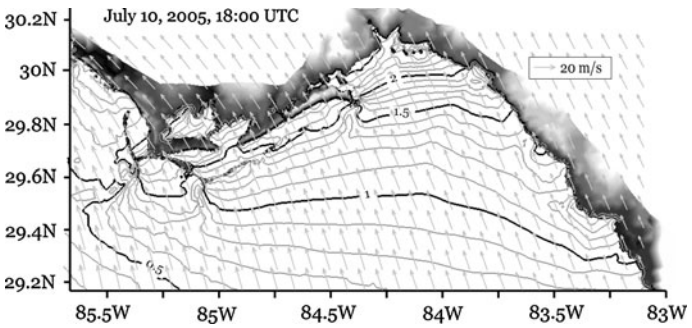


**Fig. 2** Model sea-level contours from the FVCOM Apalachee Bay high-resolution model at 18:00 UTC 10 July 2005, with overlaid wind vectors. *Black* contours are drawn every 0.5 m of the sea level; *gray* contours are every 0.1 m

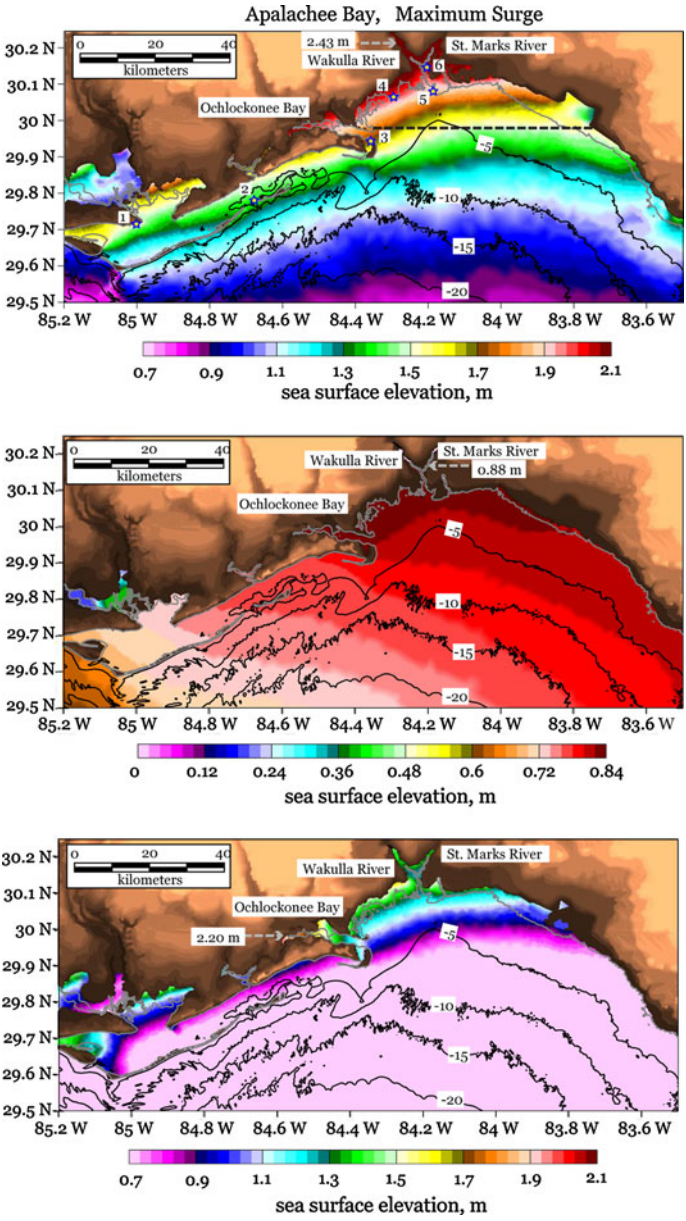


**Fig. 3** Maximum storm surge relative to MSL simulated in the Apalachee Bay model. *Black* contours are isobaths, and the coastline at MSL is marked by the *gray curve*. *Top*: Simulation with full forcing. *Blue-contoured stars* indicate locations of tide predictions: 1—Apalachicola; 2—Dog Island; 3—Bald Point; 4—Shell Point; 5—St. Marks River entrance; 6—Town of St. Marks. The *dashed line* is the transect where the volume transport is calculated (Fig. 11). *Middle*: Simulation with no wind. *Bottom*: Simulation with wind only. Values of the maximum sea-level rise for each experiment are indicated at their locations

remotely generated sea-level anomalies propagating into the region, but does not take into account other factors that may contribute to the sea-level response to the storm. This precludes the validation of the model results with many observations, which are representative of the storm tide and include all these effects on the local sea level. One approach to this problem is to modify the storm surge simulation to numerically model the inverse barometer effects, wave setup, wave runup, and astronomical tides. An alternative approach used here, however, is to obtain the estimates of these other factors contributing to the sea level during the storm using empirical and theoretical methods. These estimates are added to the simulated storm surge to compare model results with observations.

## 4.1 Inverse barometer effect

The inverse barometer effect is estimated as (Gill 1982):

$$\eta_a = -\frac{p'_a}{\rho g}, \tag{1}$$

where $p'_a$ is the atmospheric pressure anomaly, $\rho$ is the water density, and $g$ is gravitational acceleration. Assuming that the undisturbed sea level corresponds to the climatology mean pressure, $p'_a$ is the deviation of the observed pressure from the mean value. The climatology mean of sea-level pressure over the Apalachee Bay area during July is 1018 mb (data from NOAA/OAR/ESRL PSD, Boulder, Colorado, USA, www.cdc.noaa.gov). Sea-level pressure measured at Shell Point on 10 July ranged from 1008.4 mb at 12:00 UTC to 1006.2 mb at 18:00 UTC. The water density in the coastal region is roughly 1,020 kg $m^{-3}$. Therefore, the inverse barometer effect is estimated to add O (0.1 m) of sea level to the storm surge in the area during Hurricane Dennis. Note that this is an order of magnitude less than the inverse barometer effect expected near the core of a strong storm due to the large distance between this location and the storm's landfall location.

## 4.2 Wave setup and runup

### *4.2.1 Wave setup*

Wave setup is the increase in mean water level shoreward of the breaker line due to wave breaking. When waves break, they exert a net force on a water column caused by the decrease in radiation stress (Longuet-Higgins and Stewart 1964). Gradients of radiation stress quantify a net force on a water column arising from wave breaking. Based on Longuet-Higgins and Stewart (1963) in a quasi-steady state and neglecting the wave energy dissipation, the cross-shore component of the radiation stress is balanced by the cross-shore ($x$ direction) gradient of the sea level ($\bar{\eta}$):

$$\rho g d \frac{\partial \bar{\eta}}{\partial x} = -\frac{\partial S_{xx}}{\partial x}, \tag{2}$$

where $\rho$ is the water density, $g$ is gravitational acceleration, $d$ is the total depth, and $S_{xx}$ is the flux in the $x$ direction of the $x$ component of wave-related momentum (radiation stress). Seaward of the breaker zone, the mean water level decreases and in the surf zone, the mean water level increases toward the shoreline. The maximum increase in the water level at the shoreline is set up. Descriptions of the methods used for estimating the wave setup and

other necessary parameters (beach slope, wind fetch, wind speed) are outlined in Appendix 1. This approach yields wave setup estimates from 0.44 to 0.54 m (Table 2).

It should be mentioned, however, that these values are derived on the basis of a very rough estimate of the beach slope (taken as 0.01). It is anticipated that the beach slope is underestimated on the seaward side of the islands and overestimated near Shell Point where bottom is very flat. For example, for a beach slope of 0.1, the wave setup would range from 0.69 to 0.85 m. A smaller slope (<0.01), which is the slope near Shell Point, has only a minor effect on the breaker index and consequently the wave setup estimate (Table 3). However, for flatter and longer beaches, ignoring dissipation may not be a valid assumption. In this case, most wave energy dissipates because of wave breaking at a greater distance from the coast. This type of beach with gentle slope is called a "dissipative beach" (Guza 1974; Sherman 2005) because of the importance of dissipation. Classification of the beach zone is determined using the surf-scaling parameter (Sherman 2005)

$$\varepsilon = \frac{H_b \kappa^2}{g\beta^2} \tag{3}$$

where $H_b$ is the wave height at incipient breaking, $\kappa$ is the wave number, and $\beta$ is the beach slope. For the slope $\beta = 0.005$ and wave estimates determined in Appendix 1 (Table 3), the surf-scaling parameter is 64.8. According to Guza (1974) and Sherman (2005), beaches where $\varepsilon$ is larger than 20 dissipate most wave energy by the wave breaking. Hence, contribution from the wave setup to the sea-level rise during the storm along the Shell Point coast is deemed to be much smaller than the estimates in Table 3.

#### *4.2.2 Wave runup*

According to Smith (2002), runup is the maximum of the instantaneous water elevation of wave uprush above the still-water level. Wave uprush, or swash, is the fluctuation in water level about the wave setup (mean water level due to wave action). Wave runup can be estimated on the basis of empirically determined functions of beach slope, incident height, and wave steepness (e.g., Hedges and Mase 2004). In this study, wave runup is omitted in the storm tide estimation because it is a poorly known quantity and observations of maximum water level are available from inside structures where this effect is negligible.

### 4.3 Tides

Local tides can strongly affect the total inundation caused by storm surge depending on whether the maximum surge occurs during high or low tide. Although tides in the Gulf of Mexico are relatively small (roughly 1 m) compared to the tidal range in the global ocean, the northern WFS, which encompasses Apalachee Bay, hosts the largest astronomical tidal range in the Gulf. (The St. Marks River has errantly been reported to have the largest tidal range in the Gulf (FDEP 2006), although amplitudes of the dominant M2, K1, and O1 constituents are slightly larger at Cedar Key, just a few kilometers southeast of the model domain shown in Fig. 1b).

Tide predictions available for several locations (shown in the upper diagram, Fig. 3) have been calculated using the XTide utility (D. Flater, "XTide"; http://www.flaterco.com/xtide/) and adjusted to a reference MSL. The simulated maximum surge in the Apalachee Bay region occurred between 18:00 (Ochlockonee Bay) and 21:00 UTC (St. Marks), (upper diagram, Fig. 4). The timing of the maximum surge is close to the peak

**Table 2** Estimates of maximum storm tide relative to MSL

| Location | Simulated local maximum surge, m | UTC time of maximum surge on July 10 | Inverse barometer | Wave setup | Tide | Storm tide | HWM ID (FEMA, 2005) | HWM coordinates | | NAVD88 correction to MSL[a] | HWM's adjusted to MSL |
|---|---|---|---|---|---|---|---|---|---|---|---|
| | | | | | | | | Lat, N | Lon, W | | |
| Apalachicola | 1.58 | 19:00 | 0.10 | 0.44–0.54 | 0.1 | 2.22–2.32 | DFLC-05-04 | 29.71 | 85.01 | −0.045 | 2.31 |
| Dog Island | 1.48 | 19:00 | 0.10 | 0.44–0.54 | 0.34 | 2.36–2.46 | DFLC-14-07 | 29.78 | 84.66 | 0.057[b] | 2.62 |
| Bald Point | 1.82 | 19:00 | 0.10 | 0.44–0.54 | 0.08 | 2.44–2.54 | DFLC-04-19 | 29.93 | 84.34 | −0.021 | 2.63 |
| Shell Point | 2.05 | 20:00 | 0.10 | 0.44–0.54 | 0.40 | 2.99–3.09 | DFLC-10-04 | 30.06 | 84.28 | −0.006 | 2.86 |
| St. Marks R. entr. | 1.95 | 20:00 | 0.10 | 0.44–0.54 | 0.55 | 3.04–3.14 | DFLC-10-03 | 30.09 | 84.16 | −0.022 | 2.86 |
| Town of St. Marks | 2.26 | 21:00 | 0.10 | 0 | 0.40 | 2.76 | DFLC-01-02 | 30.16 | 84.22 | −0.05 | 2.85 |

[a] NOAA National Ocean Service, http://tidesandcurrents.noaa.gov/

[b] Estimate from station 8728408 (East Dog Island) is used

**Table 3** Estimates of the deep-water wave and wave breaking characteristics

| Characteristics | $\beta = 0.1$ | | $\beta = 0.01$ | | $\beta = 0.005$ | |
|---|---|---|---|---|---|---|
| | $w_{10} = 20$ | $w_{10} = 25$ | $w_{10} = 20$ | $w_{10} = 25$ | $w_{10} = 20$ | $w_{10} = 25$ |
| Deep-water wave height, $H_0$, m | 3.23 | 4 | 3.23 | 4 | 3.23 | 4 |
| Deep-water wave period, $T_0$, s | 7.58 | 8.18 | 7.58 | 8.18 | 7.58 | 8.18 |
| Deep-water wave length, $L_0$, m | 89.6 | 104.28 | 89.6 | 104.28 | 89.6 | 104.28 |
| Wave height at incipient breaking, $H_b$, m | 2.93 | 3.58 | 2.93 | 3.58 | 2.93 | 3.58 |
| Breaker depth index, $\gamma_b$ | 1.17 | 1.16 | 0.82 | 0.81 | 0.78 | 0.8 |
| Depth of breaking, $d_b$, m | 2.5 | 3.08 | 3.6 | 4.4 | 3.7 | 4.5 |
| Set down at breaking point, $\eta_b$, m | −0.21 | −0.25 | −0.14 | −0.17 | −0.14 | −0.17 |
| Setup, $\eta_s$ | 0.79 | 0.95 | 0.44 | 0.54 | 0.42 | 0.52 |

of the high tide. For selected locations, high tide occurred between 20:05 and 22:07 UTC (Fig. 5). Assuming the tidal wave effect is linearly additive to the predicted storm surge, tide predictions are added to the simulated sea-level rise (Fig. 6).

The water-level time series with astronomical tides included indicate that local tides may change the timing of the high surge. For example, at Shell Point, the simulated storm surge has exceeded 1.5 m after 12:00 UTC 10 July. With the tides, this value has been exceeded almost 15 h earlier on 9 July at 21:00 UTC. This effect of shifting in time the maximum surge by a tidal wave should be considered when planning evacuation and preparedness during storms because a storm tide can exceed a particular threshold (for example, the height of a protective levee) for a given location earlier than a storm surge prediction. Hurricane Ike (September 2008) could serve as an illustration of the importance of high surge timing for evacuation planning. During Hurricane Ike, more than 200 people on the Texas Bolivar Peninsula were caught unexpectedly by flood waters exceeding 3.7 m above sea level in advance of the hurricane, covering the only evacuation road (J.C. McKinley, I. Urbina, 09/12/2008, "Huge Storm Slams Into Coast of Texas", The New York Times). Although the occurrence of the high surge along the Texas coast during Ike most likely had causes other than the tide, one may speculate that similar effects could be caused by local astronomical tides, at least in the regions where the large tide amplitudes are observed.

Another obvious detail in Fig. 6 is that because of unfortunate coincident timing, the maximum surge occurred close to the time of high tide along the Apalachee Bay coast during Hurricane Dennis, amplifying the sea-level elevation up to 0.4–0.5 m (at the St. Marks River entrance and Shell Point, for instance). Peaks of the storm surge when added to astronomical tides are still lower than the maximum sea-level rise at these locations during the hurricane, as determined by high-water marks (HWMs) (HWMs are discussed in Sect. 5.2). The wave setup and inverse barometer effect still need to be added for comparison with HWM observations.

### 4.4 Estimates of maximum storm tide

Using the values for the inverse barometer, wave setup, and tide contributions to the sea level during Hurricane Dennis, the local maximum in the sea level is estimated (Table 2)

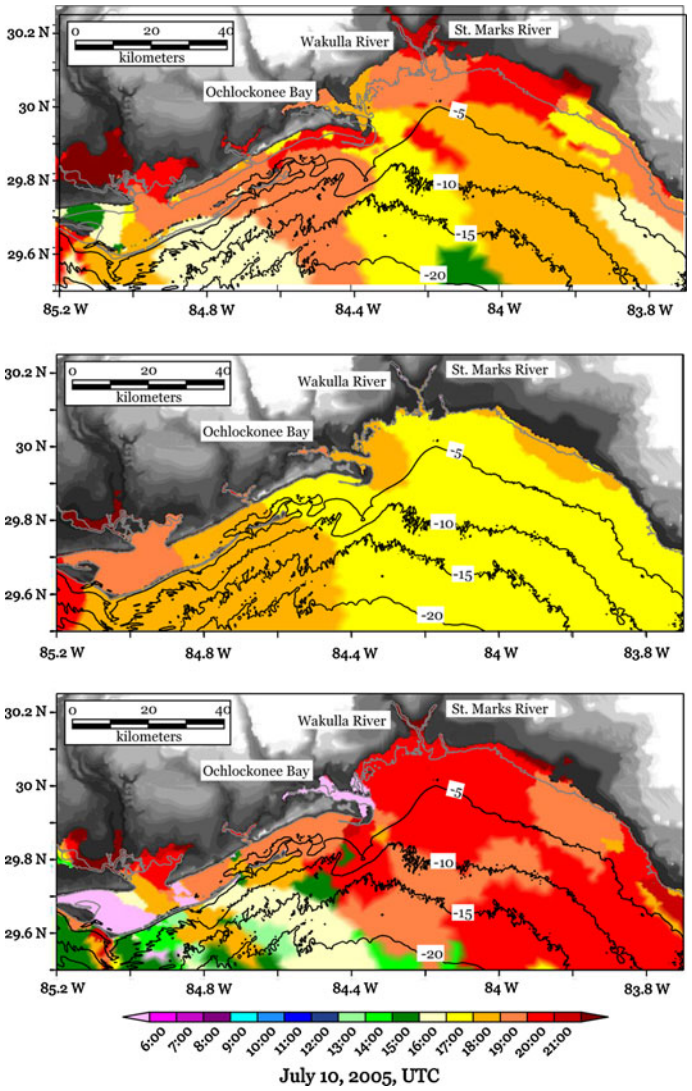


**Fig. 4** Time of simulated maximum storm surge in the Apalachee Bay model. *Top*: Simulation with wind and shelf wave. *Middle*: Simulation with no wind. *Bottom*: Simulation forced by winds only

for locations for which the tide prediction is available (shown Fig. 3, upper panel). Estimates of storm tide near the Shell Point-St. Marks area (>2 m) are greater than those in Apalachicola Bay (<2 m), consistent with the observed flooding in these areas, due to higher tides and storm surge. Wave setup at St. Marks is assumed to be zero because of its distance upriver from the coast. In the following sections, the estimates of sea-level rise during Hurricane Dennis are validated against documented sea-level rise from post-storm surveys and sea-level observations.

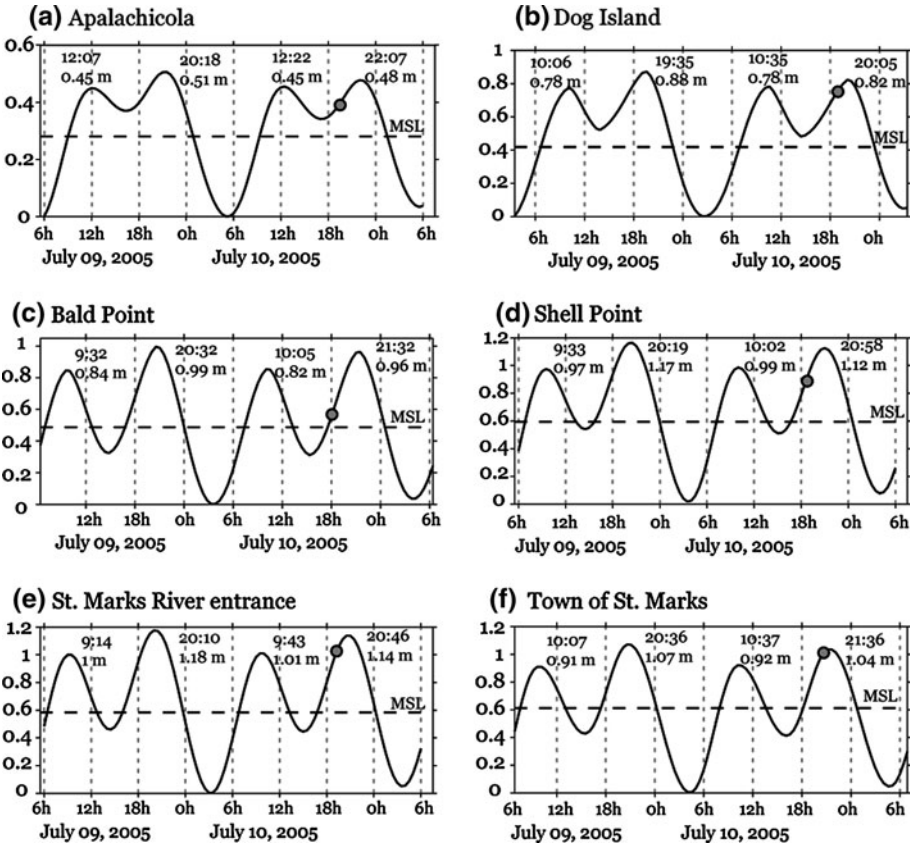


**Fig. 5** Tide predictions in Apalachee Bay. The zero of the ordinate is MLLW, and the *dashed line* is MSL. *Gray bullets* are time of the maximum storm surge in the model

## 5 Comparison with observations

### 5.1 Sea level at NOAA C-man station SHPF1

Sea-level measurements from the NOAA coastal C-MAN station at Shell Point (NDBC station SHPF1, 30°3.6′N, 84°17.4′W) are the only available coastal sea-level observations during Hurricane Dennis in the St. Marks area. The station is located in a small harbor in one of the boat channels, completely protected from the direct wave action. Thus, the wave effect is expected to be small at this site. The time series is detided and the inverse barometer effect is subtracted (0.1 m), yielding a residual sea level referenced to MSL (yellow line in Fig. 7).

Noticeably different solutions result from 3D configurations of the FVCOM Apalachee Bay model, however. Simulations with 8 (blue line in Fig. 7) and 10 $\sigma$-levels (black) simulate the peak surge very close to the observed maximum surge. Analysis of divergences in the storm surge solutions from different FVCOM model runs is presented in Sect. 7. Inspection of the sea-level time series in Fig. 7 reveals discrepancies in the timing of the simulated and observed maximum surge. The observed maximum surge at Shell Point was

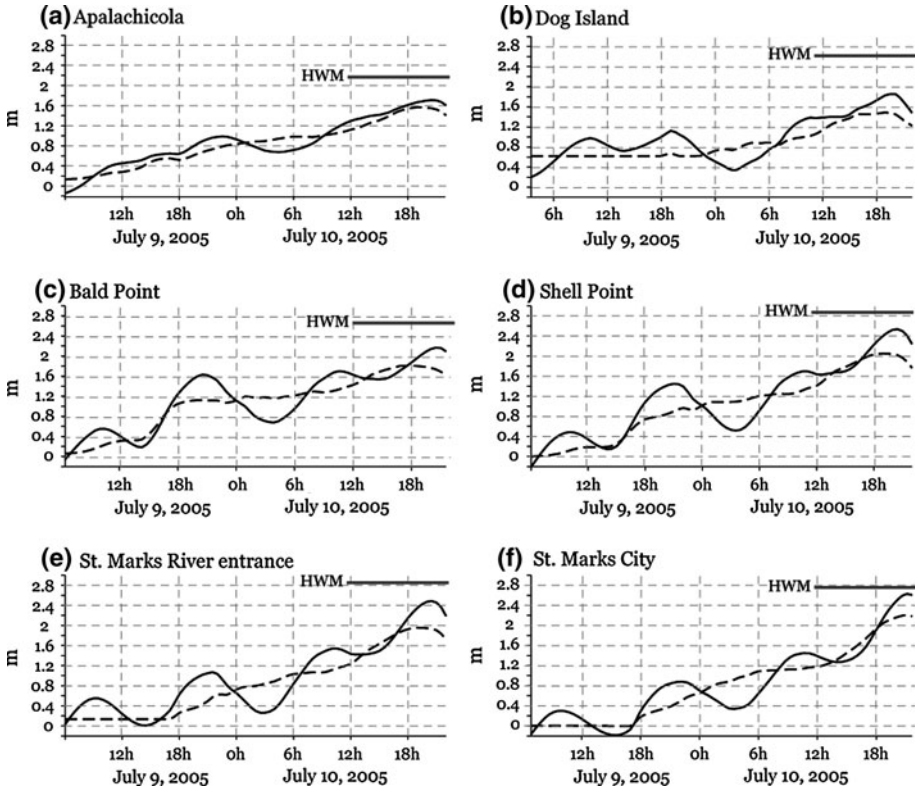


**Fig. 6** Time series of simulated storm surge (*dashed*) and storm tide (*solid*) at selected locations relative to MSL. The *gray horizontal* line indicates HWMs closest to the locations (adjusted to MSL)

2.19 m at 16:48 UTC on 10 July. From the hourly model output, the Apalachee Bay model simulates the maximum surge near that location at 19:00 UTC on the same day. Wind forcing is a probable source of errors of timing of the maximum surge in the simulation. There are very few time series of wind observations during the hurricane event in the studied region. The Shell Point station (SHPF1) used to compare sea-level time series with the model is not in an optimal location for accurate wind observations during severe storms. The station at this time was surrounded by buildings that alter wind characteristics in the proximity of the station. The other nearest station is NDBC Station SGOF1 (C-Tower, 29.41 N, 84.86 W) located about 20 miles offshore from St. George Island (Fig. 1b). Wind observations from C-Tower are used to validate the wind fields used in the model after height adjusting the measurements to 10 m (Fig. 8).

The wind fields used in the model are objectively gridded with dynamical constraints to blend NCEPR 2 and H*Wind fields (see Morey et al. (2005) for more details on the objective gridding technique). In simplified terms, the gridded wind product largely matches the high-resolution observationally derived H*Wind fields within several hundred kilometers of the center of the hurricane, and farther away, the coarser-resolution (2.5°) NCEPR 2 data are mostly used to complete the fields. Thus, one should expect that the winds in the blended wind product are more accurate near the storm than over the far field. Indeed, prior to 18:00 UTC 9 July, there are significant mismatches between the observed

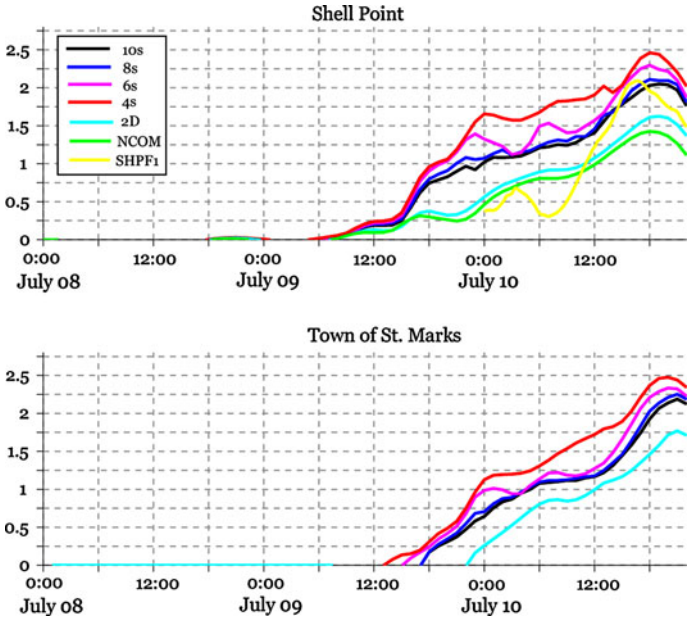


**Fig. 7** Time series of sea level (meters) relative to MSL. *Upper panel*: Sea level at Shell Point (30°3.6′N, 84°17.4′W). The *yellow line* is observed sea level at NDBC station SHPF1 without tides and inverse barometer effect (0.1 m). The *green curve* is for the Morey et al. (2006) NCOM simulation of the Gulf of Mexico during Hurricane Dennis. The *cyan line* is modeled sea level from the 2D FVCOM. The *other colors* are solutions from the 3D FVCOM with different number of vertical $\sigma$-layers. *Lower panel*: Time series of model sea level at the Town of St. Marks from 2D and 3D models (see legend in the upper diagram)

winds and the gridded wind product at the C-Tower location, and this corresponds to the time frame when the storm is far enough away that the H*Wind fields do not extend to the observation location. After 10:00 UTC 10 July, when the hurricane has approached the Apalachee Bay region (Fig. 1a), the blended wind product used to force the model represents the storm winds fairly well. Between these times, when the storm is approaching, directional errors are generally around 30° as a consequence of the poor-resolution model wind data used to complete the blended fields far from the storm center.

Following analysis of the wind fields, the wind-driven model solution is more accurate as the storm nears the region, but there are errors in the model forcing away from the storm. Thus, there may be discrepancies in the structure of the shelf wave generated in the large-scale Gulf of Mexico model due to inaccuracies in the far-field winds. The delay of the storm surge maximum at the Shell Point location in the simulation probably stems from a delay of the arrival of the long shelf wave.

### 5.2 High-water marks

The Apalachee Bay model predicts significant inundation of the coastal zone of Apalachee Bay, particularly near the Apalachicola River mouth, the back of Ochlockonee Bay, Bald Point, and in the Wakulla-St. Marks rivers area (Fig. 3). To further validate the modeled inundation, the simulation results are compared with coastal high-water marks (HWMs) collected during post-storm surveys (FEMA 2005). HWMs left on structures are the

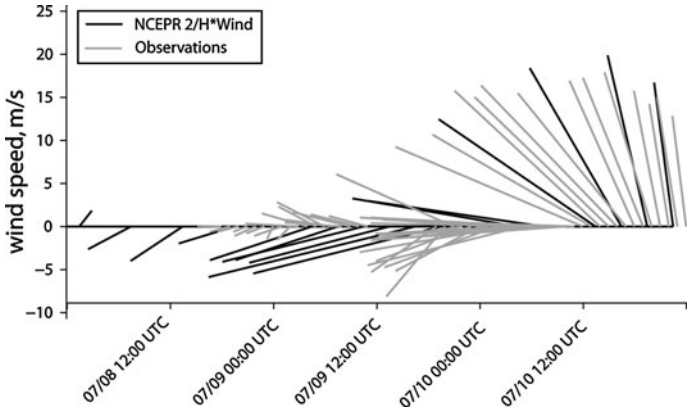


**Fig. 8** 8-min averaged wind measured at the NDBC station SGOF1, height adjusted to 10 m, and wind vectors from the same location from the NCEPR 2/H*Wind gridded wind product

primary source of data for the maximum water level during a hurricane. However, it is not straightforward to compare surge model results with the HWMs. The simulation in this study predicts only storm surge due to local wind forcing and the incoming long shelf wave. "Surge only" HWMs are taken at places protected from waves (e.g., inside buildings), so the effect of wave runup is excluded. However, other factors, such as tides, inverse barometer effects, and likely wave setup, can affect the height of the marks. An additional complication is the need to establish a reference height for comparing the HWMs with the model. For the purposes here, the NAVD88-referenced HWMs are adjusted to MSL. Finally, the accuracy and quality of these measurements is an issue, as discussed by Luther et al. (2007). Nevertheless, HWM observations are the only data available to determine sea-level rise during the storm in areas away from the few sea-level recording stations.

HWMs in the Apalachee Bay area (Fig. 9) indicate substantial inundation along the coast in agreement with the simulation (compare with the upper diagram in Fig. 3). Estimates of storm tide from the storm surge simulation results added to estimates of inverse barometer, wave setup, and tides at specified locations (Table 2) are fairly close to the HWMs within 1–10%. The simulated sea-level maxima at locations protected from direct wave action by wide and shallow grass flats (Shell Point and St. Marks River entrance) are overpredicted compared to the HWMs by 5–9%. A possible explanation is the assumption in Sect. 4.2 that this beach is not dissipative. On the other hand, for Dog Island, wave setup may be underestimated by 0.16–0.26 m (6–10%) due to underestimated bottom slope. At St. Marks, the estimated maximum storm tide (2.76) is close to the HWM of 2.85 m. Note that wave setup is expected to be negligible at this location. Thus, it is plausible that estimates of wave setup are the largest unknown for these comparisons and a more sophisticated approach, such as coupling a suitable wave model to the surge model, may reduce this uncertainty.

## 6 Local flooding of St. Marks

The town of St. Marks, located approximately 10 km up the St. Marks River, 275 km east of the Hurricane Dennis storm track, experienced only modest (minimal tropical storm

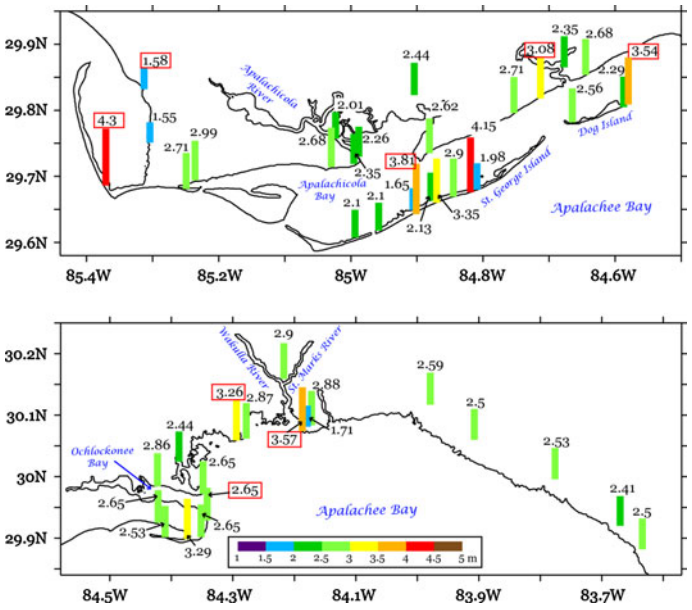


**Fig. 9** High-water marks (m) relative to NAVD88 along the Apalachee Bay coast (based on FEMA 2005). *Top*: Western part of the domain. *Bottom*: Eastern part of the domain. Values in the *red boxes* are for the HWMs affected by waves

strength) winds. However, HWMs indicate a maximum storm tide at the town exceeding 2.8 m (Fig. 9). Flooding of St. Marks and nearby areas is further documented in the "Tropical Cyclone Report" for Hurricane Dennis from the NOAA National Hurricane Center (available online: www.nhc.noaa.gov/pdf/TCR-AL042005_Dennis.pdf) and FEMA (2005), but the cause of this severe unexpected flooding has not been fully answered. FEMA (2005) states that "Strong winds … along with other unidentified oceanographic processes, contributed to the high storm surge reaching so far to the east [of the storm track]. The degree to which these forces contributed to these conditions is presently not known". Since the Apalachee Bay model with 10 $\sigma$-level configuration agrees well with HWM observations at St. Marks, it provides an opportunity to further investigate the causes of the flooding of this town and the surrounding areas.

Two additional model experiments are performed. In the first experiment, the model is as described in Sect. 2, but forced at the lateral open boundaries with the barotropic shelf wave from the Gulf of Mexico model and with no local wind forcing ("nw10-s" in Table 1). In the second experiment, the model is forced only by winds with radiation open boundary conditions ("wnd10-s" in Table 1). This eliminates the incoming shelf wave from the simulation. The purpose of these experiments is to examine the relative contributions of the large-scale sea-level anomalies and local wind-driven surge to the water-level rise within the Wakulla and St. Marks River system that was not represented in the previous study (Morey et al. 2006).

When no winds force the model, the maximum sea level occurs in the northeastern corner of Apalachee Bay with the peak value of 0.88 m less than 1 km upriver from St. Marks (middle diagram in Fig. 3). Timing of the maximum surge caused by the shelf

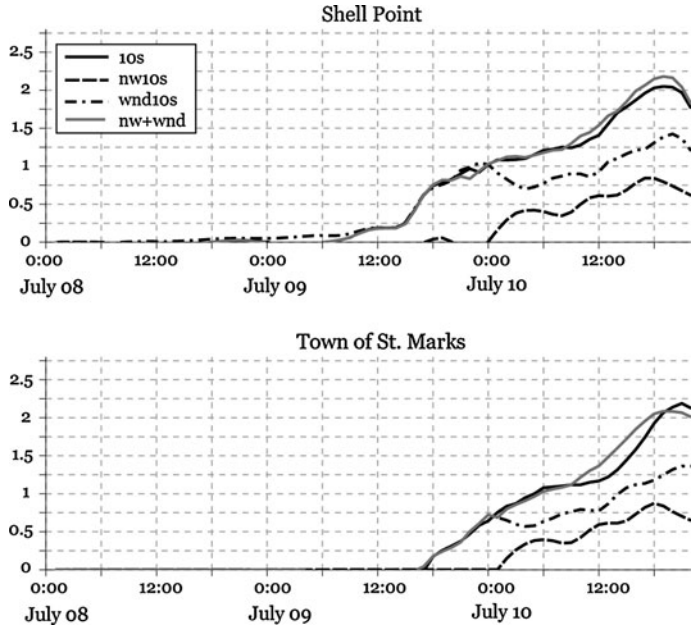


**Fig. 10** Time series of the model sea level (*top*) at Shell Point and (*bottom*) at Town of St. Marks (#6 in Fig. 3) for the 10 $\sigma$-model with full forcing (*black solid line*), with no wind forcing (*black dashed line*), and with no shelf wave forcing (*black dash-chained line*). The *gray line* shows the wind-forced model solution added to the wave-forced model solution

wave shows westward propagation of the crest with retardation of the sea-level anomaly in the river channels and bays (middle, Fig. 4). From this model experiment, the contribution of the long shelf wave to the flooding at St. Marks is 0.85 m ($\sim$30%) at 18:00 on 10 July.

From the experiment forced only by winds, the location of the maximum surge is shifted to Ochlockonee Bay (lower panel in Fig. 3). Timing of the maximum wind surge is within 1–2 h after the arrival of the shelf wave crest (lower panel in Fig. 4). The maximum of the shelf wave is wide and spread over 2–3 h. For example, at Shell Point and the town of St. Marks, local peaks of the wind surge and shelf wave crest do not exactly coincide in time (Fig. 10). At both locations, the wind surge peaks 3 h after the shelf wave crest has passed. However, the sea level has receded only 6% over this time and the shelf wave contributes 35% (town of St. Marks)—38% (Shell Point) to the simulated storm surge with full forcing (Fig. 10). The maximum modeled surge occurs during the rising phase of the local tides (Fig. 5), and at the St. Marks River entrance and the town of St. Marks, the maximum surge is very close to the tidal peak. This contributes an additional 0.4–0.5 m ($\sim$15%) of the total sea-level rise.

Thus, the model experiments suggest that during Hurricane Dennis, the timing of the maximum surge at the town of St. Marks was a result of the arrival of the sea-level anomaly from the long shelf wave nearly coincident with the maximum wind-driven local surge. Unfortunately for the residents of St. Marks, high tide occurred at nearly the same time (21:22 UTC) as the maximum storm surge and added $\sim$0.4 m (14%) to the storm tide. Had these factors not occurred nearly coincidentally, the flooding would not have

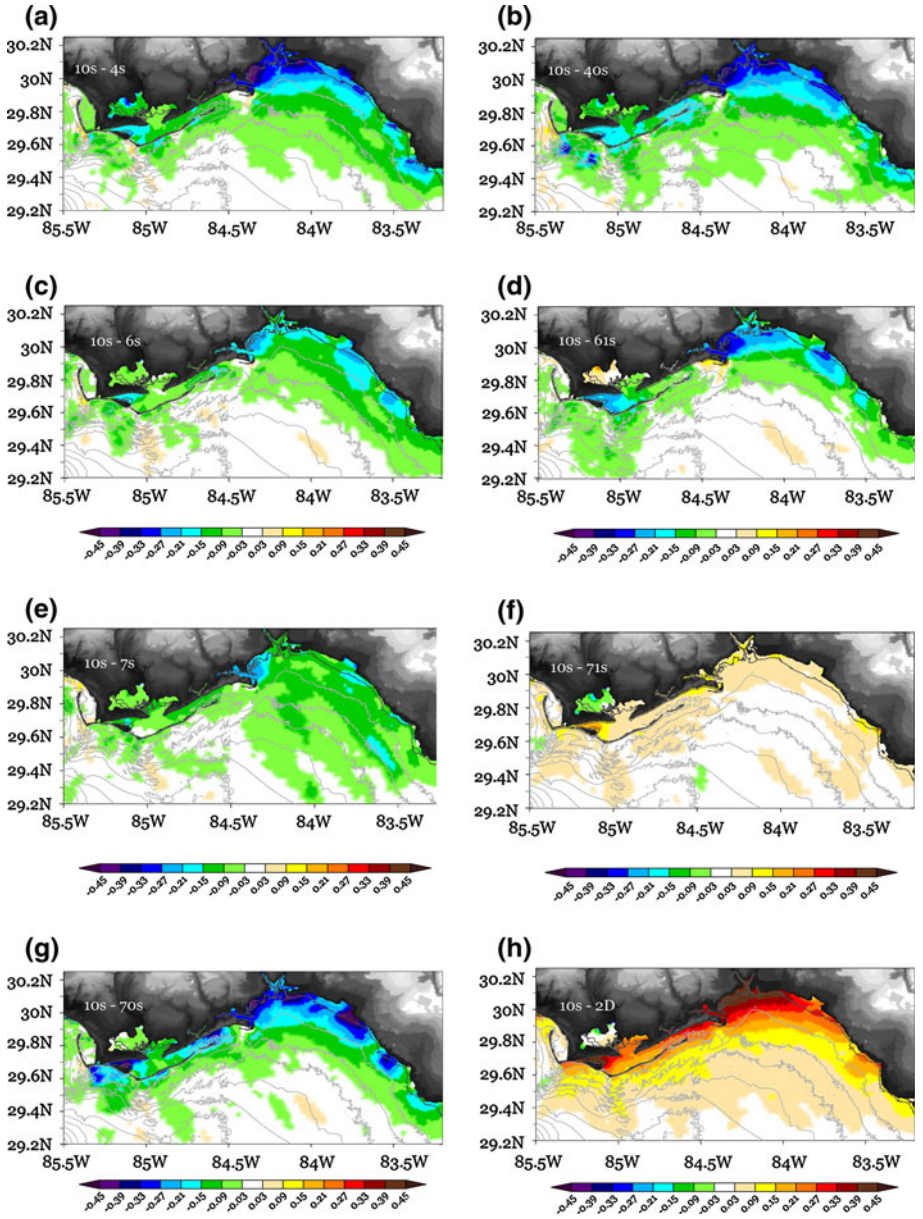


**Fig. 11** Differences in the maximum storm surge simulated in different model experiments. **a** "10-s"–"4-s"; **b** "10-s"–"40-s"; **c** "10-s"–"6-s"; **d** "10-s"–"61-s"; **e** "10-s"–"7-s"; **f** "10-s"–"71-s"; **g** "10-s"–"70-s"; **h** "10-s"–"2D". Positive values mean larger storm surge in the 10 $\sigma$-model

been so devastating for the town. For example, if the maximum surge occurred at low tide (around 5:00 UTC), the maximum water level would have been reduced by about 1 m, or 35%.

## 7 Consequences of vertical resolution

Presently, storm surge modeling in operational and many research applications is conducted using primarily 2D models (Jelesnianski 1965; Mattocks and Forbes 2008; Rao et al. 2009). Recently, it has been shown that 3D models can have a substantially dynamically different solution, even in unstratified cases (Weisberg and Zhang 2008). However, 3D models are inherently more expensive to run than 2D models, an important consideration for operational settings. Thus, it would be useful to understand how the storm surge solution changes with increasing vertical resolution, and use this information to assess the vertical resolution necessary for accurate storm surge prediction with minimum additional computational expense.

To address this, a suite of numerical experiments is conducted (Table 1). All model runs in the experiments described in this section are forced by wind stress at the surface and sea surface elevation along the open boundaries. The number of vertical sigma levels varies from 4 to 10 and is both evenly and unevenly distributed in the experiments. Results of the experiments are compared against the 10 $\sigma$-level model solution ("10-s" in the Table) that has been validated with observations in Sect. 5.

### 7.1 2D versus 3D simulation

The storm surge is underestimated in the 2D model compared to the 3D model with 10 $\sigma$-levels (Fig. 11h). Disagreement between the solutions increases toward the coast peaking up to 0.5 m (21%) near the St. Marks River. As explained in Weisberg and Zhang (2008), differences in the bottom stress in 2D versus 3D models yield differing vertically averaged momentum balances, and thus a discrepancy in the storm surge solution.

In addition to comparing 2D and 3D solutions, the 2D FVCOM simulation is also useful for comparing to the 2D coarser-resolution structured grid NCOM simulation by Morey et al. (2006). The solution from the 2D FVCOM simulation (cyan line in the upper Fig. 7) follows closely the time series of the sea level from the NCOM simulation of Morey et al. (2006) (green line in Fig. 7). The much coarser-resolution NCOM simulation by Morey et al. (2006) underestimated the observed storm surge, but the higher-resolution FVCOM simulation shows only modest improvement. The peak surge in the 2D FVCOM simulation is 0.2 m ($\sim$10%) higher than in the NCOM simulation but still underpredicts the storm surge at this location by $\sim$0.5 m ($\sim$24%). Although dynamically the two models are similar, one might expect a greater difference in the storm surge maximum simulated in the FVCOM unstructured grid model with much finer resolution and better representation of coastal geometry. The two model simulations use different numerical solution schemes (finite-difference vs. finite-volume), horizontal grids (structured vs. unstructured), spatial resolutions near the coast [O(1.5 km) vs. O(0.1 km)], and bottom stress parameterizations which still provide very close solutions.

Comparison between 2D FVCOM and 2D NCOM model results suggest that increasing the horizontal resolution in a storm surge model improves the localization of surge peaks but does not necessarily yield an improvement in the maximum surge over the whole domain. This may be a consideration for determining the horizontal spacing required for an operational surge model in which computational expense is particularly important.

### 7.2 3D simulations with differing vertical resolution

While the increased surge height in the 3D model configuration is anticipated on the basis of previous studies, significant differences among simulations with various configurations of the vertical grid must still be understood. The maximum sea level simulated in the 4 $\sigma$-level model exceeds the 10 $\sigma$-level solution by 10–20% along the coast (Figs. 7, 11a). That is, while the 2D simulation underpredicts the storm surge, the coarse vertical resolution 3D simulations overpredict the surge, and as the number of vertical levels increases, the solution converges toward the more realistic solution obtained from the 10 $\sigma$-level configuration (convergence is evident from the subtlety of the differences in the simulations with 8, 9—not shown, and 10 vertical levels).

Besides differences in the sea-level peaks, times series (Fig. 7) reveal an earlier and more rapid rise in sea level in the 3D configurations compared to 2D FVCOM and NCOM simulations. At around 18:00 UTC 9 July, the simulated sea level rapidly increases at Shell Point. The sea-level rise is much slower in the 2D model solution. As discussed previously, two dominant components of the storm surge are the locally wind-driven sea-level rise and the remotely forced long shelf wave that propagates into the region. Examining the sea-level time series from the realistic simulation and comparing it to simulations forced by wind only and the remotely generated signal entering through the model boundaries yields a plausible possible explanation for the mismatch in timing (Fig. 10). The sea level simulated in the model forced by wind only ("wnd10-s") nearly perfectly matches the sea level from the model with full forcing ("10-s") within the time interval from 12:00 UTC 9 July through 00:00 UTC 10 July both at Shell Point and at St. Marks. Then, the solutions diverge because of the impact of the shelf wave, which is absent in the "wnd10-s" experiment. This means that the faster rate of sea-level increase is completely attributed to the wind fields used in the simulation. As discussed earlier in Sect. 5.1, wind fields are less accurate at remote outskirts from the hurricane center, which was far away from these locations at that time. Comparison with measured winds at the station SGOF1 shows stronger model wind fields during 07/09 (Fig. 8). Interestingly, the faster rate of sea-level increase does not appear in the 2D simulation (Fig. 7) forced by the same winds, allowing one to speculate that the 3D model is more sensitive and responds faster to errors in wind forcing.

The higher maximum surge in the "4-s" experiment compared to the "10-s" experiment is a result of a larger volume transport toward the coast in the coarse vertical resolution model. The cumulative volume flux integrated over the transect across Apalachee Bay (shown in Fig. 3) is 36% higher in the 4 $\sigma$-level model than in the 10 $\sigma$-level model (Fig. 12). Obviously, the different volume transport in the models is a consequence of difference in the vertical velocity structure in these two experiments. Velocity profiles sampled at an arbitrarily selected location near the transect (84.1° W, 29.8° N) illustrate this (Fig. 13). At the beginning of the simulation, when the winds are relatively light, the flow develops a sheared velocity profile with a very smooth transition from the upper to the bottom layer (left panel in Fig. 13). In shallow water, the wind stress drives the ocean, which is retarded by the bottom friction. This velocity profile appears similar to theoretical and observed velocity profiles from the studies of unstratified lakes under light wind forcing (Francis 1953; Bye 1965). Note that velocity profiles from the 10 and 4 $\sigma$-level models are similar.

After the wind strength increases, strong vertical shear develops with a very sharp transition between the upper and lower layers (middle panel in Fig. 13). The vertical velocity gradient in the shear zone in the 10 $\sigma$-level is $\sim 1.6\ s^{-1}$. The upper layer is well

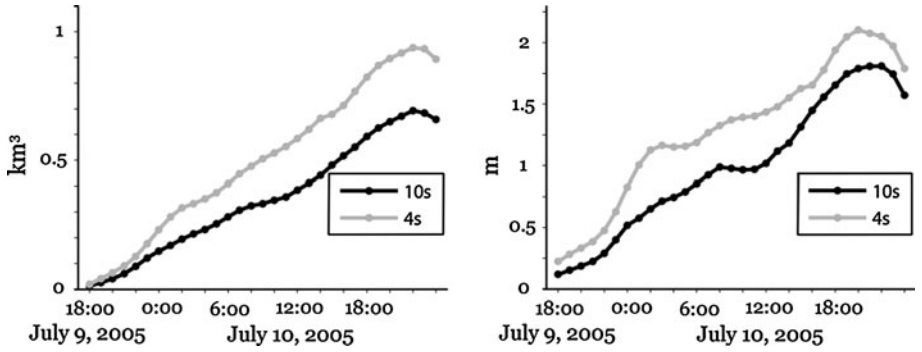


**Fig. 12** *Left*: time integrated transport ($km^3$) through the transect to Apalachee Bay from the models with 10 and 4 sigma levels. *Right*: area mean sea-level elevation in Apalachee Bay (north of the transect line) from the models

mixed because of high vertical eddy viscosity stemming from the strong storm winds. Below roughly mid-depth, the flow is much slower. In both experiments, a flow reversal occurs near the bottom driven by the pressure gradient force, which has a southward component at this location opposing the wind direction at that time.

For comparison, the velocity profile from a bottom-mounted upward-looking ADCP in the region (Station A shown in Fig. 1) is shown during a high-wind event on March 2009 at 12:00 UTC (right panel in Fig. 13). The velocity profile is the component of the velocity in the direction of the velocity vector in the bin nearest the surface, which is roughly toward the southeast. These measurements were taken during a cold-air outbreak with strong winds exceeding 20 m/s, which is comparable to the wind speed over the location shown in the middle panel of Fig. 13. A cold-air winter storm is chosen for comparison to the vertically homogeneous ocean model since these storm conditions result in nearly unstratified water at these shallow depths. The observed velocity profile has a zone of very strong shear located slightly above mid-depth that separates the flow into two layers. The upper layer has speed 3–4 times higher than the deeper layer. The vertical velocity gradient in the shear zone is $\sim 1.26\ s^{-1}$. This is very similar to the simulated two-layer flow structure in the shallow coastal region during a storm and verifies that the simulated velocity shear and two-layer structure is physically reasonable in an unstratified shallow ocean under high winds.

A noticeable feature of the velocity profiles during high winds (Fig. 13) is higher speeds and a larger velocity difference in the upper and lower layers in the 4 $\sigma$-level simulation compared to the 10 $\sigma$-level simulation. Because of the coarse vertical resolution of the 4 $\sigma$-level grid, the depth of the high shear zone is necessarily constrained to match the depth of the nearest $\sigma$-level. In this case, the upper layer is thicker than in the higher vertical resolution model. Additionally, the larger speed in the upper layer of the 4 $\sigma$-level model suggests less influence of the bottom layer on the upper layer, likely a consequence of the coarse vertical resolution. Together, these traits lead to stronger onshore transport in the coarse-resolution model and thus a higher surge. To verify this explanation, experiments are run in which the vertical grid is configured to resolve different depth ranges, including the surface layer, bottom layer, and shear zone. The experiment is described in the following section.

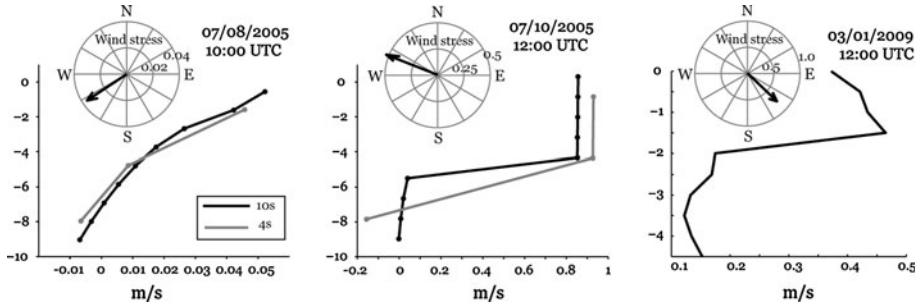


**Fig. 13** Velocity profiles projected onto wind direction. *Left* and *middle*: From 10 $\sigma$-level (*black*) and 4 $\sigma$-level (*gray*) models sampled at 84.1°W, 29.8°N. *Right*: Velocity profile from a bottom-mounted upward-looking ADCP at the NGI Station A (5 m depth) at 12:00 UTC 1 March 2009. *Insets* are wind stress vectors ($N/m^2$). The *bullets* on the *curves* indicate depths of the $\sigma$-layers

## 7.3 Resolution in different depth zones

To explore the conjecture that adequate resolution of the mid-depth high shear in shallow water under high winds is important for accurate numerical simulation of storm surge, a suite of model experiments is run with increased resolution in the upper, lower, and mid-depths (Table 1). The simulations are evaluated compared to the "10-s" model, which has been validated in Sect. 5.

Experiment "61-s" is identical to "6-s," but the distribution of $\sigma$-levels in the water column is governed by a hyperbolic tangent function such that the upper half of the water column is represented by 1 sigma layer and the rest layers are distributed in the lower water column with very high resolution near the bottom. The distribution of the vertical levels in this experiment provides the best resolution of the bottom boundary layer (the $\sigma$-layers are compacted near the bottom). However, the transition (shear) zone and the upper layer are poorly resolved. The solution from this model is not improved (not closer to the "10-s" simulation) over the "6-s" model and in fact performs worse along the coastal areas (Fig. 11c, d).

The next experiment is designed to investigate how the model performs when both bottom and surface layers are well resolved and the shear zone is not. In experiment "70-s," two thin $\sigma$-layers are placed near the surface and two are placed near the bottom. The middle depths are not resolved and the shear zone is represented by two thick layers (Table 1). The storm surge along the coast simulated in this "70-s" model configuration is larger compared to the "7-s" model, thus resulting in a worse solution than the model with evenly distributed $\sigma$-levels (compare Fig. 11e, g). Hence, degrading resolution within the shear zone for the sake of higher resolution near the surface and the bottom degrades the surge prediction along the coast.

The last of this set of experiments, "71-s," is designed such that the shear zone is well resolved but the upper and lower water columns are represented by only 1 $\sigma$-layer each (Table 1). This simulation shows markedly different results. The maximum surge is closer to the "10-s" results (compare Fig. 11e, f) than the results of the other experiments are. These results confirm that the storm surge solution is most sensitive to the vertical resolution of the shear zone and reinforce the importance of resolving the velocity profile in shallow water.

### 7.4 Sensitivity of the model solution to the bottom drag coefficient

The previous results suggest that the importance of vertical resolution in a 3-D storm surge model is to realistically represent the velocity shear seen in the model and in observations during high winds in shallow water. The remaining, and perhaps most obvious, potential impact of vertical resolution that must be investigated is its impact on bottom friction. The drag coefficient in the model is determined from a logarithmic bottom layer assumption

$$C_d = \max\left(\frac{\kappa^2}{\ln^2(z_{ab}/z_0)}, 0.0025\right) \tag{4}$$

where $\kappa = 0.4$ is the von Karman constant, $z_{ab}$ height above the bottom, $z_0 = 10^{-3}$ is the bottom roughness parameter. The formulation of the bottom drag coefficient, $C_d$, in the model is such that it is smaller in a model with coarser vertical resolution. It would be logical to suggest that the smaller coefficient explains higher velocities in the "4-s" experiment compared to "10-s."

The model "40-s" is configured identically to the "4-s" model but with a spatially dependent $C_d$ field identical to the 10 $\sigma$-level ("10-s") model (Table 1). The maximum storm surge values do not change noticeably from the "4-s" model to the "40-s" model (compare Fig. 11a, b). The "40-s" model still overpredicts the storm surge compared to the "10-s" results. Thus, the change in the bottom drag coefficient due to increasing vertical resolution manifests only a subtle effect on the model solution, compared to the impact of vertical resolution on resolving the velocity shear.

## 8 Concluding discussion

The high-resolution surge model of Apalachicola Bay based on the unstructured grid FVCOM of Chen et al. (2003) has been applied to hindcast the Hurricane Dennis case in the northeastern Gulf of Mexico. The model in a 3D configuration with 10 $\sigma$-levels has demonstrated an obvious improvement in the storm surge simulation during Hurricane Dennis compared to the previous model study by Morey et al. (2006). Small-scale processes (propagation of waves in the river channels and funneling effects) that are crucial in predicting the flooding in the St. Marks area are resolved. Inundation of the coastal area is realistically simulated and compares well with the spatial distribution of flooding and maximum sea-level rise based on HWMs (FEMA 2005). For model validation against observations, estimates of wave setup derived from empirical and analytical relations, tide elevations, and inverse barometer effect have been added to the simulated storm surge. Reconstructed total sea-level rise from the model results is within 1–10% of the maximum surge derived from the HWM observations. Validation analysis suggests that wave effect is the most uncertain factor contributing to the total sea-level rise. It is speculated that contribution from wave setup is minor for the shallow and flat coastal region, while for the coast with steeper bottom profile, wave setup may be a significant contributor to the surge. Tide contribution to the maximum surge level is estimated to be about 10–20% for the studied case. The inverse barometer effect is minor (3–5%) because of the remote location of the bay relative to the hurricane center. The model experiments reveal that unexpected flooding in Apalachee Bay was due to the coincidental arrival of the long shelf wave, high tides, and maximum local wind surge.

Experiments with different vertical discretization of the model have demonstrated high sensitivity of the model solution to the vertical grid. The 2D experiment has shown little improvement in the surge forecast compared to the coarser-resolution model of Morey et al. (2006). The maximum surge is underpredicted in the 2D model in agreement with previous studies (e.g., Weisberg and Zhang 2008). 3D simulations demonstrate convergence of the storm surge solution to the control "10-s" experiment as the number of $\sigma$-levels increases.

A counterintuitive result has been shown by the models with few vertical levels. The models with fewer $\sigma$-levels than the "10-s" run persistently overpredict the sea-level rise along the coast. Analysis of the flow vertical structure has indicated a possible reason proven by the followed model experiments. Under the strong winds, a two-layer flow develops over the shallow regions with a very strong shear in the vertical velocity profile. The sensitivity model experiments have confirmed that the storm surge solution is sensitive to the vertical resolution of the shear zone and is less sensitive to the resolution near the surface and the bottom. Experiments with modified bottom drag coefficient have demonstrated only a subtle effect on the model solution, compared to the impact of vertical resolution of the velocity shear.

**Acknowledgments** This work was supported by funding through the NOAA Applied Research Center grant to COAPS and by a grant from the Florida Catastrophic Storm Risk Management Center. Special thanks to Dr. J. Shewchuk (UC Berkeley) for providing the code of the triangular mesh generator "Triangle" and to Dr. C. Chen (UMass Dartmouth) for his assistance with FVCOM. NCEP-Reanalysis 2 data were obtained from the NOAA/OAR/ESRL PSD, Boulder, Colorado, USA, from their Web site at http://www.cdc.noaa.gov/. Sea level and wind observations are from the NOAA National Data Buoy Center; observations of the ocean currents are from the NOAA NGI Station A. Drs. M. Powell (NOAA AOML) and M. Bourassa (FSU) helped with preparing wind fields used in this study. The authors acknowledge Meredith Field and Kathy Fearon (COAPS FSU), for helping with materials on FEMA high-water mark survey and editing the manuscript. The authors thank HPC FSU staff for providing technical support for numerous simulations on HPC facility.

## Appendix 1. Wave setup estimation

Setup at the shoreline is given by (Smith 2002):

$$\bar{\eta}_S = \bar{\eta}_b + \left(1 + \frac{8}{3\gamma_b^2}\right)^{-1} H_b, \tag{5}$$

where $\bar{\eta}_b$ is setdown, $\gamma_b$ is the breaker depth index, and $H_b$ is the wave height at incipient breaking. Setdown for regular waves can be estimated from (Longuet-Higgins and Stewart 1963):

$$\bar{\eta}_b = -\frac{1}{8}\frac{H_b^2 \kappa}{\sinh(2\kappa d_b)}, \tag{6}$$

where $\kappa$ is the wavenumber and $d_b$ is the water depth at breaking. The breaker depth index is

$$\gamma_b = \frac{H_b}{d_b}. \tag{7}$$

Another important index that relates the wave height at incipient breaking and the wave height over the deep water, $H_0$, is the breaker height index:

$$\Omega_b = \frac{H_b}{H_0}. \tag{8}$$

The breaker indices Eqs. 7 and 8 depend on beach slope, which can be estimated as an average bottom slope from the break point to one wavelength offshore (Smith 2002), and characteristics of the wave (Weggel 1972; Smith and Kraus 1991). Detailed surveys of the surf zone are necessary for measuring this parameter as the available bathymetric data are not of sufficiently fine resolution. Wang et al. (2006) measured the beach slope ($\beta$) at St. George Island to be 0.05–0.06, but it is expected to be <0.01 over mud and seagrass flats near the St. Marks River entrance and Shell Point. The following wave setup estimates are derived for the beach slope of 0.01.

For calculating wave setup, characteristics of the waves generated by a storm in deep water are required. Ideally, measurements of the wave height and period from buoys could be used for estimating the wave setup. Unfortunately, there are no wave measurements available over the northern WFS during Hurricane Dennis. Therefore, Young's model (Young 1988) for fetch-limited waves is used to estimate the deep-water wave height ($H_0$) and the spectral peak period of the wave ($T_0$):

$$H_0 = 0.0016\frac{w_{10}^2}{g}\left(\frac{gF}{w_{10}^2}\right)^{0.5} \tag{9}$$

$$T_0 = 0.045\frac{2\pi w_{10}}{g}\left(\frac{gF}{w_{10}^2}\right)^{0.33} \tag{10}$$

where $w_{10}$ is 10-m wind speed and F is wind fetch.

Wind fetch is estimated on the basis of the procedure outlined in Resio et al. (2002). Away from the coast, fetch is defined such that wind direction variations do not exceed 15 degrees and wind speed variations do not exceed 2.5 m $s^{-1}$ from the mean. If distance to the upwind coastline is smaller than the fetch, the coastline limits the fetch. Estimates of wind fetch (Fig. 14) have been obtained when the hurricane center is close to Apalachee Bay when the winds reach their local maximum over the Bay. There is uncertainty about what region should be considered for estimating deep-water wave characteristics. In this study, the following logic has been used to define the region (shown in Fig. 14) where deep-water waves traveling to Apalachee Bay are generated. One criterion is the region should be deeper than the half-length of the wind waves generated during the storm. Wind waves generated during a storm in this region are O(100 m); thus, the deep region is deeper than the 100-m isobath. Another criterion is that the waves should travel to Apalachee Bay. It is assumed that the peak wave direction matches the local wind direction. The maximum surge at the Apalachee Bay coast occurred between 19 and 21 UTC (Fig. 4), about 3–4 h after the time shown in Fig. 14. Over this time, a gravity wave can travel about 200–300 km (assuming the average depth to be 50 m). From the above discussion, a possible region of deep-water generation is identified (Fig. 14). Over this region, the wind field exhibits very low curvature of the wind streamlines, resulting in a long fetch in the range from 80 to 120 km with an average of 100 km.

Wind fields used in the model experiment reveal that the maximum sustained wind over the WFS during Hurricane Dennis was in the range 20–25 m $s^{-1}$ in agreement with FDEP (2006). The maximum sustained wind measured in this area (NOAA NDBC, buoy 42036, 28°30′0″N 84°31′0″W, location is shown in Fig. 14) was 23.5 m $s^{-1}$. Therefore, Eqs. 9 and 10 estimate that deep-water wave height in the studied region is in the range from 3.2 to 4.04 m and wave period is from 7.6 to 8.2-s.

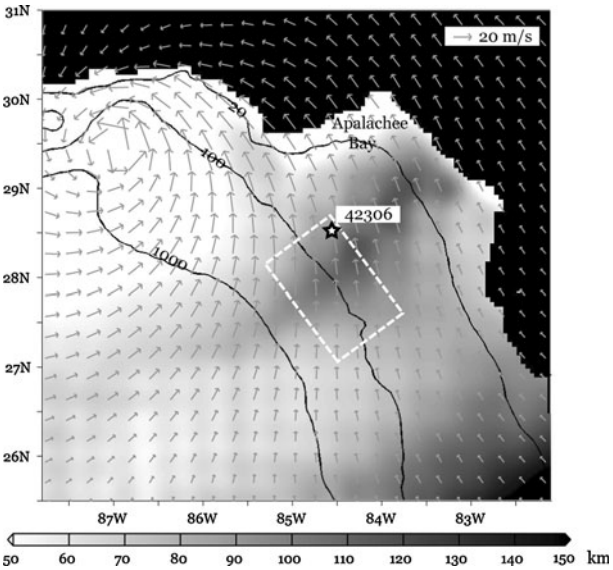


**Fig. 14** Wind fetch (km) estimated by the method of Resio et al. (2002). The wind field used for estimating the fetch is shown by the overlaid vectors. The location of NOAA NDBC station 42036 is shown. Anticipated region where deep-water waves that travel to the Apalachee Bay region are generated is marked by the *white dashed box*

Analytically derived estimates of the deep-water wave characteristics can be compared with simulated wave fields at 18:00 UTC 10 July 2005, (closest instant to the time shown in Fig. 14), from the regional North Atlantic Hurricane (NAH) NOAA WAVEWATCH III model (http://polar.ncep.noaa.gov/waves) shown in Fig. 15. The deep-water waves are considered to be the waves in the water at least 100 m depth. On the basis of the simulated significant wave direction, a possible region from where deep-water waves could travel to

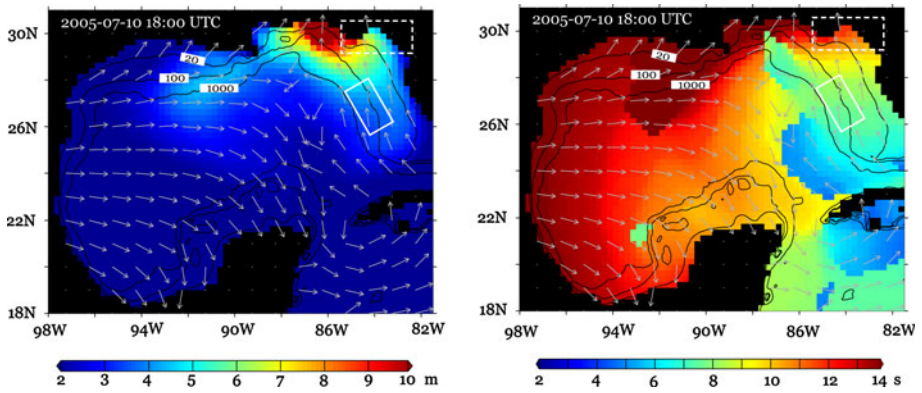


**Fig. 15** Significant wave height (*left*) and peak wave period (*right*) on July 10, 2005, at 18:00 UTC, from the regional NAH WaveWatch III wave prediction model of NOAA National Weather Service. *Overlaid gray arrows* are significant wave direction vectors. The *dashed box* roughly delineates the Apalachee Bay model domain. The *solid box* indicates anticipated region from where deep-water waves might have travelled to Apalachee Bay by the time of maximum storm surge

Apalachee Bay and contribute to the wave setup during the maximum storm surge (2–4 h later) is identified (marked by the white solid box in Fig. 15). Note that location of the area agrees with the earlier defined area for wind fetch. In this area, the significant height of the deep-water wave is 3.5–5 m with the period of 8–9-s. The analytical estimates of the deep-water wave height and period are close to the characteristics of the simulated waves. It is noteworthy that the region of maximum wave heights is not in the model domain. According to NAH simulation, on that date and time, waves greater than 10 m height with the period of 10-s were to the west of the Apalachicola Bay and did not contribute to the wave setup along the coast of Apalachee Bay.

Wave length is derived from the approximate dispersion relation for the surface gravity wave (Eckart 1952):

$$L_0 \approx \frac{gT^2}{2\pi}\sqrt{\tanh\left(\omega^2\frac{d}{g}\right)}, \tag{11}$$

where $\omega$ is wave frequency and $L_0$ is the length of the deep-water wave. The estimated deep-water wave length generated by Hurricane Dennis in Apalachee Bay is 90 m to 104 m.

The breaker height index is estimated as (Munk 1949):

$$\Omega_b = 0.3\left(\frac{H_0}{L_0}\right)^{-1/3}, \tag{12}$$

which, together with Eq. 8, gives the wave height at incipient breaking to be from 2.9 to 3.6 m. Following Weggel (1972), for regions with slopes less or equal than 0.1 and $H_0/L_0 < 0.06$, the breaker depth index is found as:

$$\gamma_b = b - a\frac{H_b}{gT^2} \tag{13}$$

where a and b are empirically determined functions of the beach slope:

$$\begin{aligned} a &= 43.8[1 - \exp(-19\beta)] \\ b &= 1.56[1 + \exp(-19.5\beta)]^{-1} \end{aligned} \tag{14}$$

The breaker depth index is 0.81. With this, Eq. 7 provides the depth of breaking from 3.6 to 4.4 m. After substituting all required values into Eqs. 5 and 6, one gets the estimated setup from 0.44 to 0.54 m.

## References

As-Salek JA (1998) Coastal trapping and funneling effects on storm surges in the Meghna Estuary in relation to cyclones hitting Noakhali-Cox's Bazar Coast of Bangladesh. J Phys Oceanogr 28:227–249

Bye JAT (1965) Wind-driven circulation in unstratified lakes. Limnol Oceanogr 10(3):451–458

Chen C, Liu H, Beardsley RC (2003) An unstructured grid, finite-volume, three-dimensional, primitive equations ocean model: application to coastal ocean and estuaries. j atmos ocea techn 20:159–186

Chen CS, Beardsley RC, Cowles G (2006) An unstructured grid, finite-volume coastal ocean model: FVCOM user manual. SMAST/UMASSD University of Massachusetts-Dartmouth, Technical report-06–0602. New Bedford, Massachusetts

Chen C, Huang H, Beardsley RC, Liu H, Xu Q, Cowles G (2007) A finite volume numerical approach for coastal ocean circulation studies: comparisons with finite difference models. J Geophys Res 112(C03018):34. doi:10.1029/2006JC003485

Eckart C (1952) The propagation of gravity waves from deep to shallow water. National bureau of standards. Circular 20:165–173
FDEP (2006) Hurricane Dennis and Hurricane Katrina. Final report on 2005 hurricane season impacts to Northwest Florida, Florida department of environmental protection division of water resource management bureau of beaches and coastal systems, Florida
FEMA (2005) Hazard mitigation Technical assistance program contract N0. EMW-2000-CO-0247, task orders 403 & 405, Hurricane Dennis rapid response Florida coastal high water mark (CHWM) collection, FEMA-1595-DR-FL, final report, 19 Dec 2005. Federal emergency management agency, region IV, Atlanta, GA
Francis JRD (1953) A note on the velocity distribution and bottom stress in a wind-driven water current system. J Mar Res 12:93–98
Gill A (1982) Atmosphere-ocean dynamics. Academic Press Inc, New York
Guza RT (1974) Excitation of edge waves and their role in the formation of beach cusps. Dissertation, University of California
Hedges TS, Mase H (2004) Modified Hunt's equation incorporating wave setup. J Waterway Port Coastal Ocean Eng 130(3):109–113. doi:10.1061/(ASCE)0733-950X
Jelesnianski CP (1965) A numerical calculation of storm tides induced by a tropical storm impinging on a continental shelf. Mon Wea Rev 93:343–360
Jelesnianski CP (1970) Bottom stress time history in linearized equations of motion for storm surges. Mon Weather Rev 98:462–478
Large WG, McWilliams JC, Doney SC (1994) Oceanic vertical mixing: a review and a model with nonlocal boundary layer parameterization. Rev Geophys 32:363–403
Longuet-Higgins MS, Stewart RW (1963) A note on wave set-up. J Mar Res 21:4–10
Longuet-Higgins MS, Stewart RW (1964) Radiation stress in water waves, a physical discussion with application. Deep-Sea Res 11:529–563
Luther ME, Merz CR, Scudder J, Baig SR, Pralgo LJ, Thompson D, Gill S, Hovis G (2007) Water level observations for storm surge. Marine Technol Soc J 41(1):35–43
Mattocks C, Forbes C (2008) A real-time, event-triggered storm surge forecasting system for the state of North Carolina. Ocean Model 25(3-4):95–119. doi:10.1016/j.ocemod.2008.06.008
Mellor GL, Yamada T (1982) Development of a turbulence closure model for geophysical fluid problem. Rev Geophys Space Phys 20:851–875
Morey SL, Bourassa MA, Davis XJ, O'Brien JJ (2005) Remotely sensed winds for episodic forcing of ocean models. J Geophys Res 110:C10024
Morey SL, Baig S, Bourassa MA, Dukhovskoy DS, O'Brien JJ (2006) Remote forcing contribution to storm-induced sea level rise during Hurricane Dennis. Geophys Res Lett 33(19):L19603
Munk WH (1949) The solitary wave theory and its applications to surf problems. Ann N Y Acad Sci 51:376–462
Murty TS (1984) Storm surges - meteorological ocean tides. Friesen Printers Ltd., Ottawa
Nihoul JCJ (1977) Three-dimensional model of tides and storm surges in a shallow well mixed continental sea. Dyn Atmos Oceans 2:29–47
Platzman GW (1958) A numerical computation of the surge of June 26, 1954, on Lake Michigan. Geophysica 6:407–438
Powell MD, Houston SH, Amat LR, Morisseau-Leroy N (1998) The HRD real-time hurricane wind analysis system. J Wind Engineer Indust Aerodyn 77(78):53–64
Rao AD, Jain I, Ramana Murthy MV, Murty TS, Dube SK (2009) Impact of cyclonic wind field on interaction of surge–wave computations using finite-element and finite-difference models. Nat Hazards 49(2):225–239. doi:10.1007/s11069-008-9284-9
Resio DT, Bratos SM, Thompson EF (2002) Meteorology and wave climate. In: Vincent L, Demirbilek Z (eds) Coastal engineering manual part II, hydrodynamics, engineer manual 1110–2-1100, updated 2006, US. Army Corps Engineers, Washington
Sherman D (2005) Dissipative beaches. In: Schwartz ML (ed) Encyclopedia of coastal science. Springer, The Netherlands, pp 389–390
Shewchuk JR (2002) Delaunay refinement algorithms for triangular mesh generation. Comput Geom 22(1–3):21–74
Smagorinsky J (1963) General circulation experiments with the primitive equations I. The basic experiment. Mon Wea Rev 91:99–164
Smith JM (2002) Surf zone hydrodynamics. In: Vincent L, Demirbilek Z (eds) Coastal engineering manual part ii, hydrodynamics, engineer manual 1110–2-1100, updated 2006, US. Army Corps of Engineers, D.C

Smith ER, Kraus NC (1991) Laboratory study of wave-breaking over bars and artificial reefs. J Waterway Port Coastal Ocean Eng 117(4):307–325

Wang P, Kirby JH, Haber JD, Horwitz MH, Knorr PO, Krock JR (2006) Morphological and sedimentological impacts of Hurricane Ivan and immediate poststorm beach recovery along the northwestern Florida barrier-island coasts. J Coastal Research 22(6):1382–1402

Weggel JR (1972) Maximum breaker height. J Waterways Harbor Coast Eng Div 98(WW4):529–548

Weisberg RH, Zhang LY (2008) Hurricane storm surge simulations comparing three-dimensional with two-dimensional formulations based on an Ivan-like storm over the Tampa Bay, Florida region. J Geophys Res 113(C12):C12001. doi:10.1029/2008JC005115

Weisberg RH, Zheng L (2006) Hurricane storm surge simulations for Tampa Bay. Estuaries Coasts 29(6A):899–913

Welander P (1957) Wind action on a shallow sea: some generalizations of Ekman's theory. Tellus 9:45–52

Young IR (1988) Parametric hurricane wave prediction model. J Waterways Harbor Coast Eng Div 114(5):637–652